ESD-TR-67-331

Technical Report

436

S. D. Weiner

Short-Pulse Scattering by a Hemisphere

18 July 1967

Prepared for the Advanced Research Projects Agency
under Electronic Systems Division Contract AF 19(628)-5167 by

Lincoln Laboratory

MASSACHUSETTS INSTITUTE OF TECHNOLOGY

Lexington, Massachusetts

The work reported in this document was performed at Lincoln Laboratory, a center for research operated by Massachusetts Institute of Technology. This research is a part of Project DEFENDER, which is sponsored by the U.S. Advanced Research Projects Agency of the Department of Defense; it is supported by ARPA under Air Force Contract AF 19(628)-5167 (ARPA Order 498).

MASSACHUSETTS INSTITUTE OF TECHNOLOGY

LINCOLN LABORATORY

SHORT-PULSE SCATTERING BY A HEMISPHERE

S. D. WEINER

Group 41

TECHNICAL REPORT TR-436

18 JULY 1967

LEXINGTON MASSACHUSETTS

ABSTRACT

The radar scattering by a conducting hemisphere for incidence along the symmetry axis has been determined as a function of frequency, bistatic angle, and polarization. From this frequency domain information, the short-pulse response is constructed using Fourier synthesis. The range resolution thus afforded permits identification of various contributions to the scattering – in particular, that due to edge diffraction. Results obtained from the geometrical theory of diffraction are in qualitative agreement with those obtained here.

Accepted for the Air Force
Franklin C. Hudson
Chief, Lincoln Laboratory Office

CONTENTS

SHORT-PULSE SCATTERING BY A HEMISPHERE

I. INTRODUCTION

The electromagnetic scattering from finite targets may often be explained as the coherent sum of returns from individual scattering centers. For example, the scattering from a sphere consists of specular and creeping-wave contributions. The known behavior of a scattering center on a simple target may be applied to a similar scattering center on a more complex target which is not amenable to analytical solution. For the nose-on backscattering from a cone-sphere,[1,2] the tip and joint returns given by the physical-optics approximation, combined with the creeping-wave return for a sphere, yield results in good agreement with experiment.

Another scattering center of interest is the edge, found on cylinders and flat-backed cones, which is usually treated using the geometrical theory of diffraction.[3] This involves the application of a two-dimensional theory to a three-dimensional problem. A different approach to edge scattering is obtained by considering the exactly soluble problem of scattering by a hemisphere. It is assumed that the edge contribution to the hemisphere scattering is representative of other rectangular edge scatterers.

In this report, the scattering by a conducting hemisphere for incidence along the symmetry axis (nose-on) is determined as a function of frequency, bistatic angle, and polarization. In general, the resulting scattering patterns are complex and difficult to interpret. Using the short-pulse response obtained from the frequency domain response by Fourier synthesis, individual contributions of each scattering center may be resolved. Once these returns are located and identified, the CW scattering is more easily interpreted.

The remainder of the report is devoted to consideration of individual scattering centers. The behavior of each return as a function of frequency, bistatic angle, and polarization is obtained and compared with that predicted using other techniques. Particular emphasis is given to edge diffraction, where the present results are compared with those given by the geometrical theory of diffraction.

II. SCATTERING BY A HEMISPHERE

The formal solution for the CW scattering from a conducting hemisphere of radius R was obtained by Kennaugh[4] in 1950 and will only be outlined here. Kennaugh's solution applies for arbitrary angles of incidence and scattering, but except in special cases, it is not suitable for numerical computation. In this report, we treat only the case of nose-on incidence, for which his results simplify considerably.

The origin is chosen so that the spherical and flat surfaces of the hemisphere have constant coordinate values $r = R$ and $\Theta = \pi/2$, respectively (Fig. 1). The space external to the hemisphere

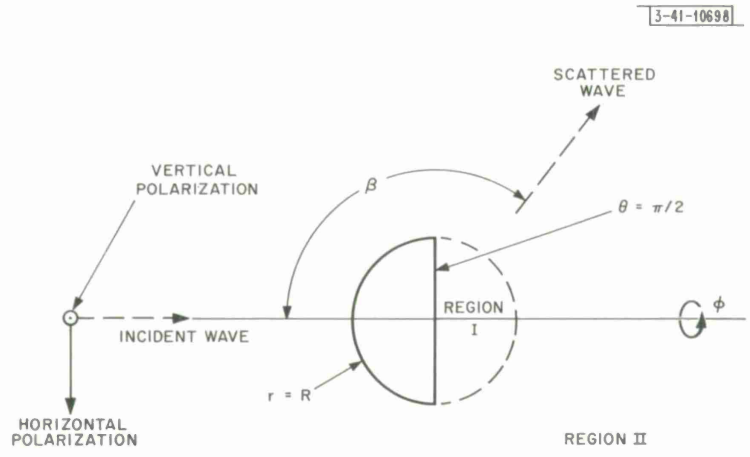

Fig. 1. Geometry of hemisphere scattering.

is then separated into two regions, with different eigenfunction expansions for the electromagnetic fields in each region. The electric field in both regions must satisfy the vector Helmholtz equation

$$(\nabla^2 + k^2)\,\vec{E} = 0 \quad , \quad k = 2\pi/\text{wavelength} \tag{1}$$

and may be expanded in terms of spherical harmonics and spherical Bessel and Hankel functions. The incident wave propagating along the z-axis (symmetry axis) contains only the first azimuthal modes (spherical harmonics of order one), and symmetry of the surface implies that only these modes will occur in the scattered fields. Without loss of generality, we further assume the incident wave is polarized in the x-direction.

In region I ($r < R$; $\Theta > \pi/2$), the electric field expansion must remain finite at the origin and satisfy the boundary conditions $E_r = E_\varphi = 0$ on the flat surface of the hemisphere, $\Theta = \pi/2$. Such an expansion is

$$\begin{aligned}\vec{E}_I = {} & \hat{r}\cos\varphi \sum_n \Gamma_{2n}\,\frac{2n(2n+1)}{kr}\,j_{2n}(kr)\,P^1_{2n}(\cos\Theta) \\ & + \hat{\Theta}\cos\varphi \sum_n \gamma_{2n-1} j_{2n-1}\,\frac{P^1_{2n-1}}{\sin\Theta} + \Gamma_{2n} j^*_{2n}\,\frac{dP^1_{2n}}{d\Theta} \\ & - \hat{\varphi}\sin\varphi \sum_n \gamma_{2n-1} j_{2n-1}\,\frac{dP^1_{2n-1}}{d\Theta} + \Gamma_{2n} j^*_{2n}\,\frac{P^1_{2n}}{\sin\Theta}\end{aligned} \tag{2}$$

where the star on some of the spherical Bessel functions denotes the operation $[d/d(kr) + 1/(kr)]$ on the function. The coefficients γ_{2n-1} and Γ_{2n} will be determined by the requirement that $\vec{E}$ be continuous from region I to region II.

In region II ($r > R$), the total E-field is the sum of the incident and scattered fields

$$\vec{E}_{II} = \hat{r}\cos\varphi \sum_n \frac{n(n+1)}{kr}\,(b_n j_n + d_n h_n)\,P^1_n$$

$$+ \hat{\theta} \cos\varphi \sum_n (a_n j_n + c_n h_n) \frac{P_n^1}{\sin\theta} + (b_n j_n^* + d_n h_n^*) \frac{dP_n^1}{d\theta}$$

$$- \hat{\varphi} \sin\varphi \sum_n (a_n j_n + c_n h_n) \frac{dP_n^1}{d\theta} + (b_n j_n^* + d_n h_n^*) \frac{P_n^1}{\sin\theta} \qquad (3)$$

with $a_n = i^n (2n + 1)/n(n + 1) = i\, b_n$. The spherical Hankel functions are those corresponding to outgoing waves. The scattering coefficients c_n and d_n are determined by requiring the electric and magnetic fields in region II to satisfy boundary conditions $E_{tan} = 0$ on the spherical surface of the hemisphere ($r = R$, $\theta < \pi/2$) and to be continuous across the boundary surface $r = R$, $\theta > \pi/2$. The first step in this process involves projecting combinations of Eqs. (2) and (3) with associated Legendre polynomials to convert the differential equations to systems of algebraic equations. These are then combined to yield the following matrix equation for the c_n, d_n in terms of the known a_n, b_n

$$\left.\begin{aligned} \sum_m C_{n,m} c_m + A_{n,m} a_m = 0 \\ \sum_m D_{n,m} d_m + B_{n,m} b_m = 0 \end{aligned}\right\} \quad \text{all } n \qquad (4)$$

with

$$A_{n,m} = m(m + 1)\,[2M_{m,m} j_m \delta_{n,m} - j_m^* N_{n,m}^{odd}]$$

$$B_{n,m} = m(m + 1)\,[2M_{m,m} j_m^* \delta_{n,m} - j_m N_{n,m}^{even}]$$

$$C_{n,m} = m(m + 1)\,[2M_{m,m} h_m \delta_{n,m} - h_m^* N_{n,m}^{odd}]$$

$$D_{n,m} = m(m + 1)\,[2M_{m,m} h_m^* \delta_{n,m} - h_m N_{n,m}^{even}]$$

$$N_{n,m}^{even} = \sum_p (M_{2p,n} M_{2p,m} / M_{2p,2p})\,(j_{2p}^* / j_{2p})$$

$$N_{n,m}^{odd} = \sum_p (M_{2p-1,n} M_{2p-1,m} / M_{2p-1,2p-1})\,(j_{2p-1} / j_{2p-1}^*)$$

$$M_{n,m} = \int_{\pi/2}^{\pi} P_n^1 P_m^1 \sin\theta\, d\theta = M_{m,n}$$

$$= n(n + 1)/(2n + 1) \quad ; \quad m = n$$

$$= 0 \quad ; \quad m + n \text{ even},\ m \neq n$$

$$= \frac{(-1)^{(m+n+1)/2}}{(n - m)(n + m + 1)} \frac{(n + 1)\, m(m + 1)\, (n + 1)!\, m!}{2^{m+n+1} [(\frac{n + 1}{2})!\, (\frac{m}{2})!]^2} \quad , \quad n \text{ odd},\ m \text{ even} \ .$$

(interchange n and m for n even, m odd)

In the above equations, the spherical Bessel and Hankel functions are evaluated at kR.

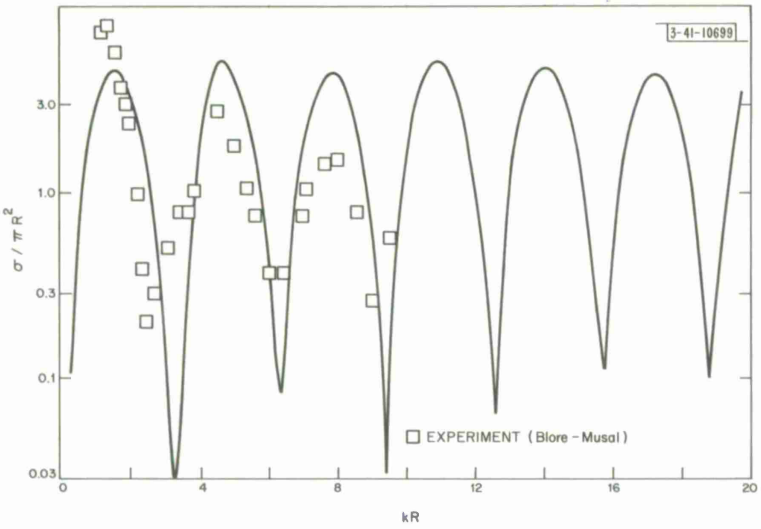

Fig. 2. Backscattering from hemisphere.

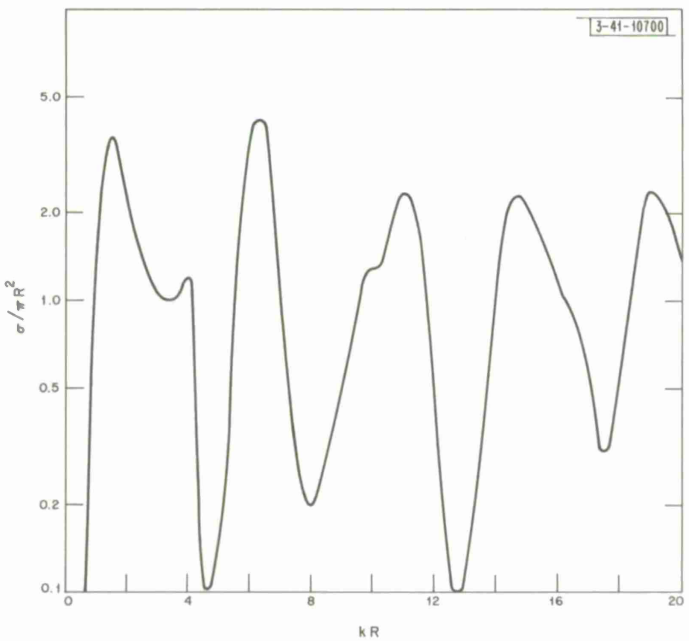

Fig. 3. Scattering from hemisphere; $\beta = 30°$, HH polarization.

If only a finite number of equations and terms in each equation is retained, Eqs. (4) may be solved numerically for the c_n and d_n. From numerical computation, typically the number of terms required for convergence is of the order of 1.6 kR. Once the c_n and d_n have been determined, the scattered field is obtained from Eq. (3).

Knowledge of the scattered electric field vector for all Θ and φ is sufficient to specify the scattering matrix. For simplicity, consideration will be restricted to the principal polarization basis for which the scattering matrix is diagonal. The two polarizations considered correspond to E-plane scattering where the incident and scattered electric fields are in the plane of scattering defined by the incident and scattering directions, and H-plane scattering where the incident and scattered electric fields are perpendicular to the plane of scattering.[5] If the plane of the transmitter, target, and receiver is taken as the horizontal plane, E-plane scattering corresponds to HH polarization while H-plane scattering corresponds to VV polarization. This is indicated in Fig. 1. In terms of the scattered electric field, the scattering amplitudes for various polarizations are given by

$$A_{HH}(\beta) = \sqrt{4\pi r^2}\, E_{\Theta}^{sc} \quad (\Theta = \beta,\ \varphi = 0)$$

$$A_{VV}(\beta) = \sqrt{4\pi r^2}\, E_{\varphi}^{sc} \quad (\Theta = \beta,\ \varphi = \pi/2) \quad . \tag{5}$$

The radar cross section is given by $\sigma = |A|^2$. We may note from Eq. (3) that for the case of backscattering ($\beta = 0$), the HH and VV amplitudes are identical and hence will not be distinguished.

Numerical solutions to Eqs. (3) through (5) have been obtained for values of kR from 0.2 to 20 in steps of 0.2, for β from 0° to 150° in steps of 30°, and for both HH and VV polarization. Calculations were not performed for $kR > 20$ due to excessive computer time and storage requirements. The radar cross section normalized to πR^2 is presented as a function of kR for backscattering ($\beta = 0°$) in Fig. 2 and for $\beta = 30°$, HH polarization, in Fig. 3. Also shown in Fig. 2 are experimental points obtained by Blore and Musal.[6] The theoretical backscattering cross section is an oscillatory function of kR and could be interpreted as resulting from interference between two scattering centers with individual cross sections of the order of πR^2. As shown in Sec. IV, there are actually two strong and two weaker contributions to the backscattering from the hemisphere. The cross section for $\beta = 30°$ in Fig. 3 is considerably more complicated and difficult to interpret in the frequency domain. However, in the time domain, the interpretation simplifies considerably. The technique used to obtain the short-pulse response is outlined in the following section.

III. SHORT-PULSE RESPONSE

As indicated in Figs. 2 and 3, the scattering by a hemisphere is a complicated function of frequency. Interpretation of these results may be simplified by using the notion of scattering centers.[3] Interference between rays having different optical paths has been evoked to explain the frequency dependence of scattering from various targets.[1,2] The usefulness of this technique is somewhat restricted, however, due to the difficulty in identifying individual returns on complicated targets from data in the frequency domain. By considering the scattering in the time domain, the problem simplifies due to the temporal resolution of returns having different optical paths. By calculating the scattering of appropriate short-pulse incident signals, it is possible to obtain a sequence of scattered pulses, each corresponding to a distinct scattering

center. In practice, this technique is limited by the separation and frequency dependence of individual returns, the pulse width used, and the accuracy and extent of data in the frequency domain. Examples of the use and limitations of short-pulse scattering are described in subsequent sections.

Given the frequency dependence of the hemisphere scattering amplitude A(kR) as calculated in the previous section, it is possible to construct the scattering of a short-pulse signal using Fourier synthesis. Since A(kR) was calculated only for discrete values of kR, it is necessary to use a Fourier series representation rather than a Fourier transform. This causes no difficulty since Fourier transforms performed numerically are in reality Fourier series. After presenting the series used for short-pulse synthesis, we will consider the consequences of this finite sampling.

An incident signal may be written in the time domain as

$$E^{in}(t) = \sum_n E(\omega_n) \exp(-i\omega_n t) \quad , \quad \omega_n = n\Omega \tag{6}$$

where Ω is the fundamental frequency in the Fourier series and $E(\omega)$ is the frequency representation of the incident signal. From Eq. (6) and knowledge of the scattering amplitude, the scattered signal may be written as

$$E^{sc}(t) = \sum_n A(\omega_n)\, E(\omega_n) \exp(-i\omega_n t) \quad . \tag{7}$$

It is useful to convert Eqs. (6) and (7) to dimensionless forms by normalizing time, distance, and frequency in terms of the hemisphere radius, R. If the electric fields are written as functions of radar range $x = ct/2$, Eqs. (6) and (7) become

$$E^{in}(x) = \sum_n E(k_n R) \exp[-2i(k_n R)\,(x/R)] \tag{8}$$

and

$$E^{sc}(x) = \sum_n A(k_n R)\, E(k_n R) \exp[-2i(k_n R)\,(x/R)] \tag{9}$$

with $k_n R = n\delta = n\Omega R/c$. The resulting signals will be periodic in x/R with period π/δ. The minimum value of δ is 0.2, determined by the calculational increment in A(kR). This provides a maximum signal period of about 15 R. A similar technique has been used by Rheinstein[7,8] in investigating the scattering by conducting and dielectric spheres. He used a smaller calculational increment to obtain signal periods greater than 50 R. This was necessary in his case due to the long optical paths of some returns. A much shorter period is adequate in the present case, as is shown in the next section. Since the incident and thus the scattered signal repeat after a distance $\pi R/\delta$, any return delayed by this distance or greater will "fold over" and appear to have a shorter delay. Such ambiguous returns can easily be recognized, however, since their location changes with changes in δ.

For the present report, a truncated Gaussian spectrum was used for E(kR), giving an incident signal in the form of a modified Gaussian pulse. In particular:

$$E(kR) = \begin{cases} \Delta \exp[-\Delta^2 (kR - k_o R)^2/2] & ; \quad |kR - k_o R| \leq 3/\Delta \\ 0 & ; \quad \text{otherwise} \end{cases} \tag{10}$$

where Δ is the pulse width in units of R and $k_o R$ is proportional to the center or carrier frequency. The resulting incident signal is calculated using Eq. (8). In Fig. 4, $|E^{in}|^2$ is graphed as a function of x/R for $\delta = 0.4$, $\Delta = 0.4$, $k_o R = 8$. The sidelobe level is determined by the truncation point used in Eq. (10) and is below any expected return. Using Eqs. (9) and (10), the scattered field may be calculated. In Figs. 5 through 7, $|E^{sc}|^2$ normalized to πR^2 is graphed as a function of x/R for bistatic angles of 0°, 30°, and 120°. This is equivalent to an A-scope presentation of the detected power. Various returns are identified and will be discussed in more detail in subsequent sections.

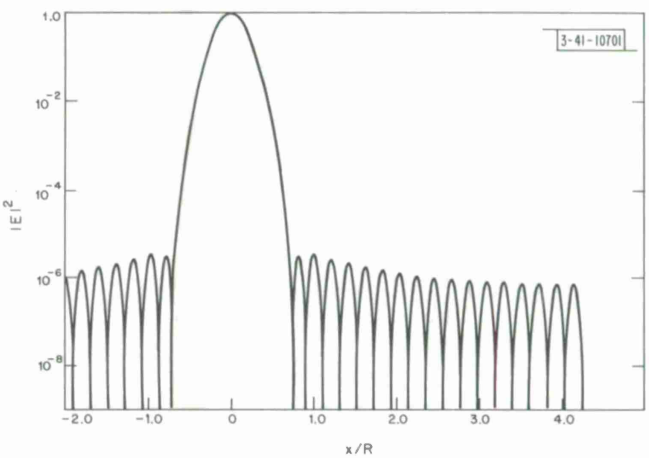

Fig. 4. Incident pulse shape.

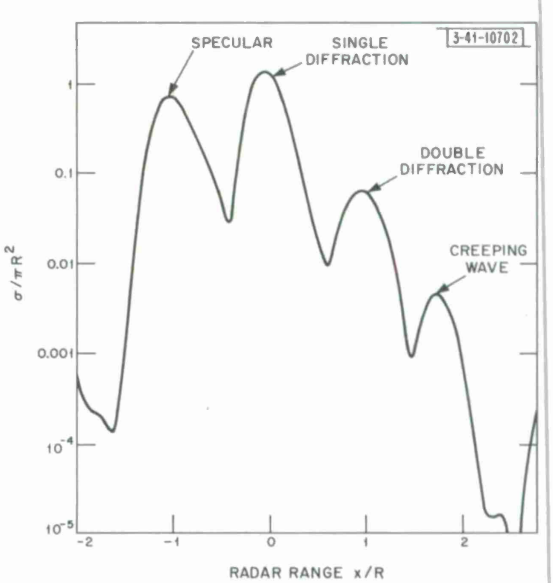

Fig. 5. Short pulse response of hemisphere; $\beta = 0°$, $k_o R = 8$.

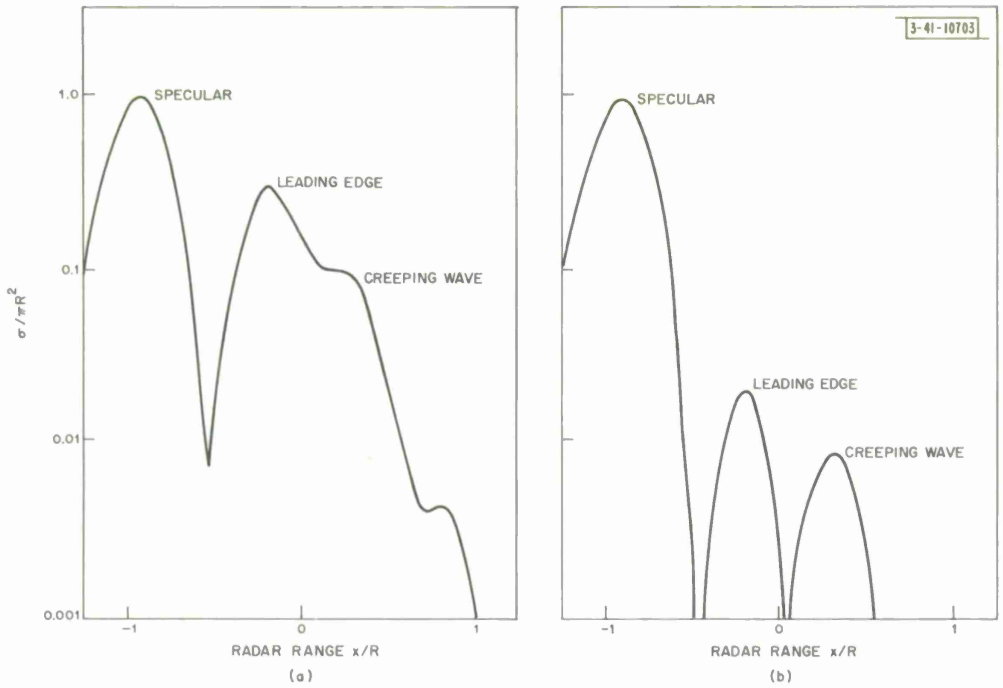

Fig. 6. Short pulse response of hemisphere. (a) $\beta = 30°$, $k_oR = 8$, HH polarization. (b) $\beta = 30°$, $k_oR = 8$, VV polarization.

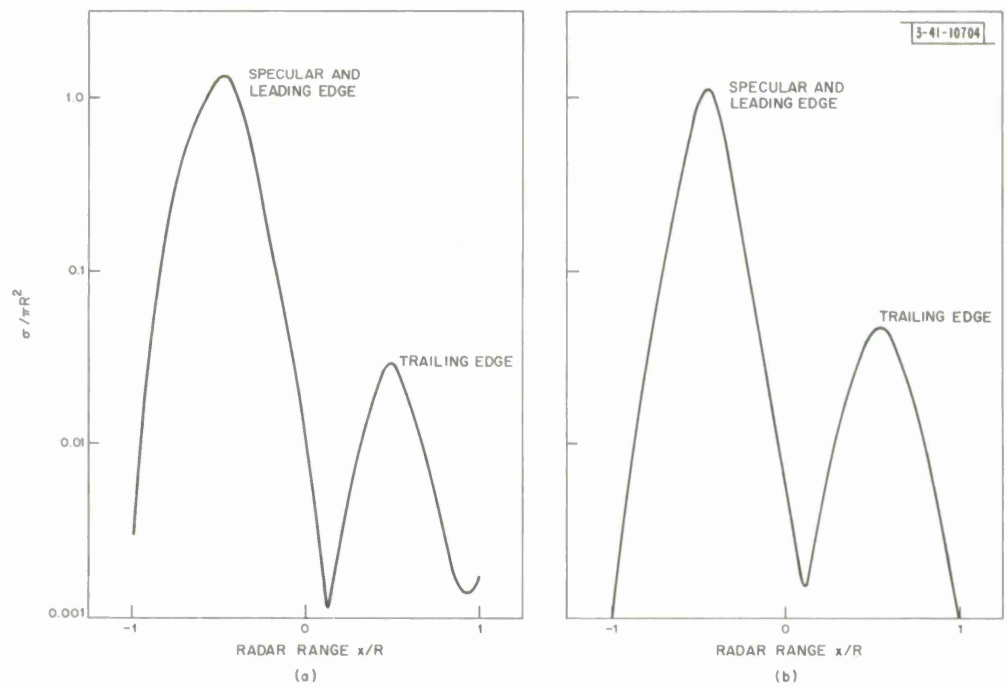

Fig. 7. Short pulse response of hemisphere. (a) $\beta = 120°$, $k_oR = 8$, HH polarization. (b) $\beta = 120°$, $k_oR = 8$, VV polarization.

IV. RAY PATHS

A ray path is defined as a line connecting the transmitter, target, and receiver which is of stationary (usually minimum) length. Such paths include direct rays, specularly reflected rays, edge diffracted rays, and surface rays.[9] As an example of ray paths on a hemisphere, Fig. 8 presents the first four contributions to the backscattering return along with the corresponding radar ranges. It should be noted that the creeping-wave path shown in Fig. 8 differs from what will be called the creeping wave for bistatic scattering (Fig. 9). The four resolved returns indicated in Fig. 8 are clearly evident in the short-pulse backscattering response given in Fig. 5. This time domain presentation should be contrasted with the frequency domain presentation given in Fig. 2. Use of the time domain solution permits direct identification of both large and small contributions having different optical path lengths. Although Fig. 5 represents the case kR = 3, a sequence of short-pulse responses for varying center frequencies can show the behavior of individual scattering returns as a function of frequency. Before presenting results for individual returns, we will consider some of the ray paths for bistatic scattering.

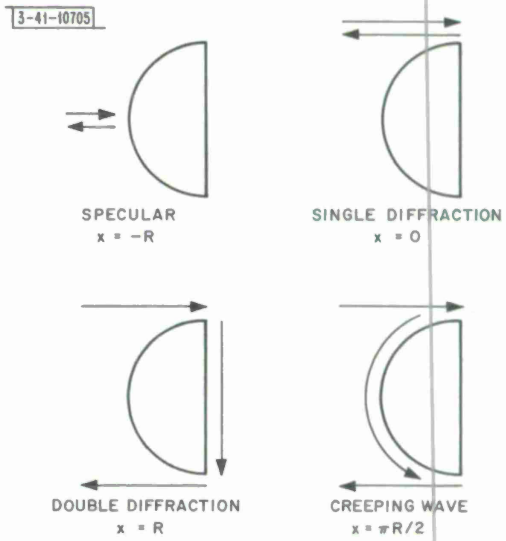

Fig. 8. Backscattering ray paths.

For the case of backscattering, all ray paths contributing to a given scattering center return have the same radar range. This is no longer true for bistatic scattering, as may be seen in Fig. 1. A ray scattered by the upper part of the hemisphere edge travels less distance than a ray scattered by the lower part. Thus, bistatic scattering permits resolution of isolated portions of the edge scatterers. Table I and Fig. 9 show the ray path and radar range for all returns undergoing two or less edge diffractions. These returns include one specular, three singly-diffracted, and six doubly-diffracted rays. Figure 10 presents a graph of radar range for these returns as a function of bistatic angle. Additional rays are undergoing three or more edge diffractions which may precede some of the rays considered over certain ranges of β. For example, there is a triply-diffracted return which occurs at $x/R = 2.0$ for $\beta = 0°$ and then joins smoothly to the curve for ray path 6 at $\beta = 90°$. The backscattering returns shown in Fig. 8 are evident at $\beta = 0°$ in Fig. 10. Note that for bistatic scattering, ray path 4 is called the creeping wave. Figure 10 shows that for certain values of β, two or more ray paths have the same radar range. In these cases, it will be impossible to resolve or identify the individual returns.

At this point, it is necessary to describe the technique used for obtaining the returns from individual scattering centers. In this section we consider only backscattering, although the same technique was used to obtain the bistatic results presented in the following sections. By calculating σ as a function of x for a variety of center frequencies and pulse widths, knowledge of the short-pulse contribution of individual scattering centers may be obtained. Thus, the nose-on short-pulse backscatter from a cylinder or flat-backed cone is expected to have components analogous to the singly- or doubly-diffracted waves on the hemisphere. However, these results cannot be used directly to predict the contribution of individual scattering centers to the CW

TABLE I

RAY PATHS ON HEMISPHERE

No.	Name	Bistatic Angles	No. of Edge Diffractions	Surface Waves		Radar Range (in Units of R)
				Spherical Surface	Flat Surface	
1	Specular	0 – 180	0	No	No	$-\cos(\beta/2)$
2	Leading Edge	0 – 180	1	No	No	$-(\sin\beta)/2$
3	Trailing Edge	90 – 180	1	No	No	$(\sin\beta)/2$
4	Creeping Wave	0 – 180	1	Yes	No	$\beta/2$
5	Double Diffraction	0 – 180	2	No	Yes	$1-(\sin\beta)/2$
6		90 – 180	2	No	Yes	$1+(\sin\beta)/2$
7		0 – 180	2	Yes	No	$(\pi-\sin\beta)/2$
8		90 – 180	2	Yes	No	$(\pi+\sin\beta)/2$
9		0 – 180	2	Yes	Yes	$1+\beta/2$
10		0 – 180	2	Yes	No	$(\pi+\beta)/2$

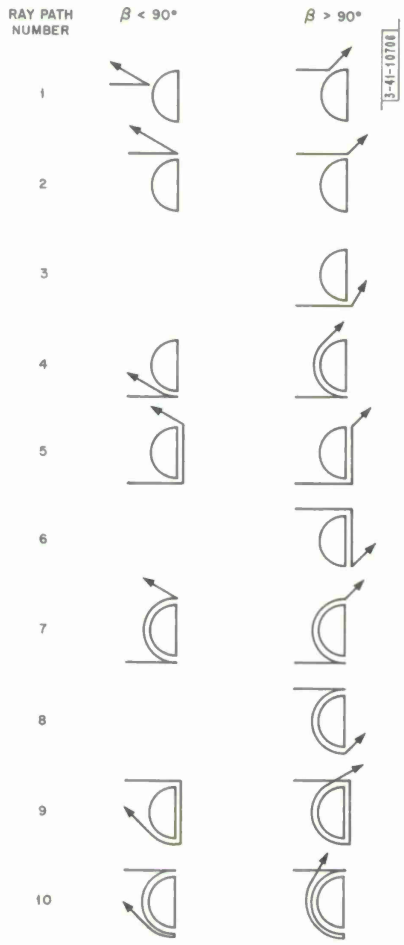

Fig. 9. Bistatic scattering ray paths.

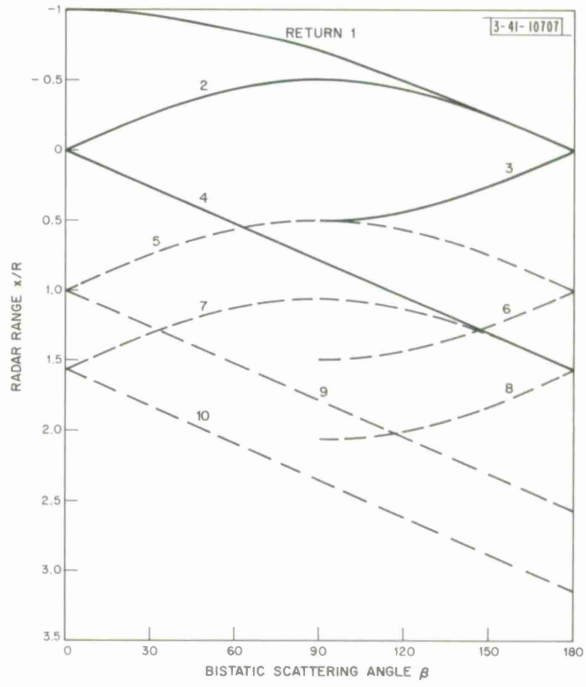

Fig. 10. Radar range as a function of bistatic angle.

amplitude. Rheinstein[8] obtained the CW amplitudes of the specular and creeping-wave returns from a sphere by separating the short-pulse response into two distinct contributions and transforming each contribution separately back to the frequency domain (equivalent to a Watson transform). This was possible because these two returns were completely resolvable due both to their separation ($R + \pi R/2$ in radar range) and to the pulse resolution used. Unfortunately, this technique cannot be used for the hemisphere. The singly- and doubly-diffracted returns fall in the range interval between the specular and creeping wave, considerably decreasing the separation of individual returns. Furthermore, higher-resolution pulses cannot be used without determining the CW scattering amplitude for $kR > 20$. As a result, the individual returns overlap and interfere to a certain extent.

The results obtained from the short-pulse response have been moderately improved by assuming the CW scattering amplitude to have the form

$$A(kR) = \sum A_i \exp(2ikx_i) \tag{11}$$

where A_i and x_i are the amplitude and location of the i^{th} return. The x_i are chosen to correspond to the four returns under consideration, and the A_i are then determined to best fit the CW response as a function of kR. By fitting to the CW amplitude over successive small ranges of kR, the frequency dependence of individual returns may be estimated. Results for $\sigma_i/\pi R^2$, where $\sigma_i = |A_i|^2$, are presented as a function of kR in Fig. 11. It must be remembered that these numerical results are only approximate, particularly for the weaker scatterers. Several features of these results may be noted. The specular return is fairly close to the optics value $\sigma/\pi R^2 = 1$ and is roughly independent of kR. The increase in the specular return at low frequency[8] cannot be observed using the present technique. The singly-diffracted return is approximately a factor of two larger than the value $\sigma/\pi R^2 = 16/27$ predicted by Keller's geometrical diffraction theory,[3] with both being independent of kR. Geometrical diffraction theory[3,10] predicts the doubly-diffracted return to be $\sigma/\pi R^2 = 64/9\pi kR$. The doubly-diffracted return shown in Fig. 11 is considerably weaker and decreases with kR more rapidly than 1/kR. The creeping-wave return in Fig. 11 is substantially weaker than the other three.

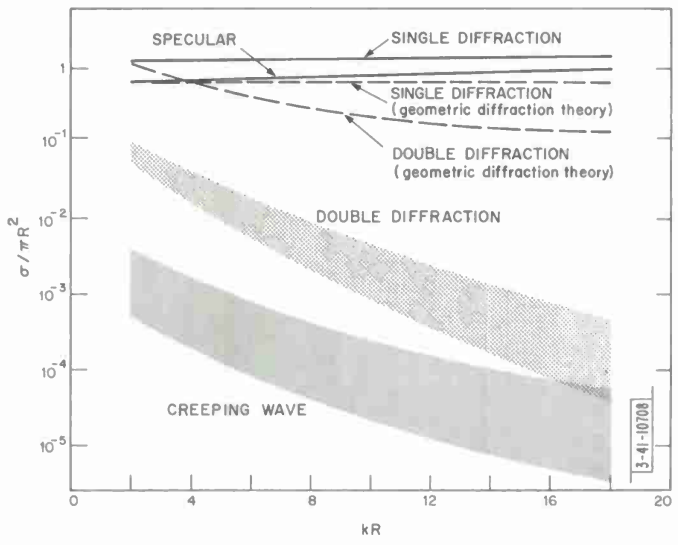

Fig. 11. Contributions to hemisphere backscattering.

The same technique is used to obtain the bistatic scattering results presented in the following sections. For each bistatic angle and polarization, an equation equivalent to Eq. (11) is solved to obtain the behavior of the three or four dominant returns. As each return is considered, the present results are compared with results obtained using a different technique. In particular, the results for edge scattering are compared with the predictions of the geometrical diffraction theory.

V. SPECULAR RETURN

The specular return which follows ray path 1 is usually the dominant contribution to the hemisphere scattering. It is predicted by geometrical and physical optics as well as by exact theory. The specular contribution for $\beta = 0°$ is shown in Fig. 11. Figure 12 presents the specular return for $\beta = 30°$, $60°$, $90°$, and $120°$ for both HH and VV polarizations. For $\beta = 150°$, the specular return cannot be resolved from the leading-edge return. The results shown in Fig. 12 may be compared with expressions for the specular return from a sphere:[11]

$$\frac{\sigma_{HH}}{\pi R^2} = 1 - \frac{14 \sin^2(\beta/2) - 1}{4(kR)^2 \cos^6(\beta/2)} + \ldots \tag{12a}$$

$$\frac{\sigma_{VV}}{\pi R^2} = 1 - \frac{14 \sin^2(\beta/2) - \cos^2\beta}{4(kR)^2 \cos^6(\beta/2)} + \ldots \tag{12b}$$

While it is clear that additional terms would be required to obtain the oscillations in Fig. 12, several features of the specular return may be explained qualitatively from the kR and β dependence indicated in Eq. (12). As kR increases, σ approaches πR^2, and the departure of σ from πR^2 increases with increasing β. The second terms in Eq. (12) are of the same order of magnitude as this departure.

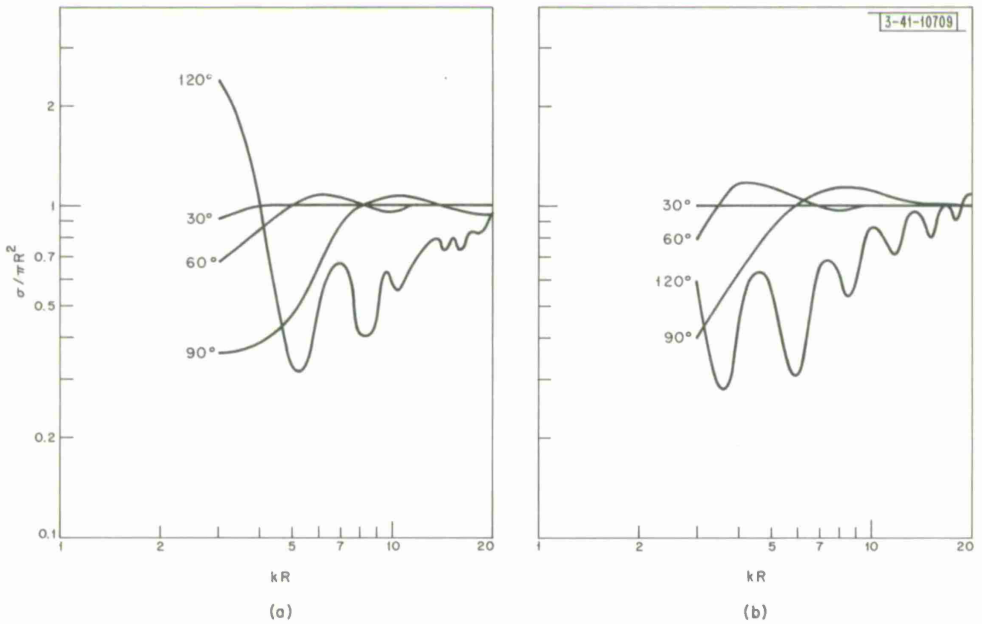

Fig. 12. Specular return. (a) HH polarization. (b) VV polarization.

VI. EDGE RETURNS

In this section we consider only the leading-edge return which follows ray path 2 and the trailing-edge return which follows ray path 3. (This exists only for $\beta \geqslant 90°$.) The doubly-diffracted contributions (ray paths 5 through 10) are generally much weaker and were included only for $\beta = 0°$. Before giving the results of the present analysis, it is of interest to consider the application of geometric diffraction theory to these returns.

Geometric diffraction theory calculates the contribution of each ray path to the scattering by combining geometric ray tracing with two-dimensional edge diffraction theory. The geometric factors and diffraction coefficients for edge scattering have been given by Keller[3,9] and Bechtel[10] as functions of the wedge angle (90° for the hemisphere), scattering angles, and radius of curvature (R). Specializing their results to the present case, we have for the leading edge

$$\frac{\sigma_{HH}}{\pi R^2} = \frac{4}{3\pi kR \sin\beta}\left[\frac{1}{2} + \cos\left(\frac{2\beta}{3}\right)\right]^{-2} \tag{13a}$$

$$\frac{\sigma_{VV}}{\pi R^2} = 0 \tag{13b}$$

and for the trailing edge

$$\frac{\sigma_{HH}}{\pi R^2} = \frac{4}{3\pi kR \sin\beta}\left[\frac{1}{2} + \cos\left(\frac{2\pi + 2\beta}{3}\right)\right]^{-2} \tag{14a}$$

$$\frac{\sigma_{VV}}{\pi R^2} = 0 \quad . \tag{14b}$$

As shown in Fig. 1, a vertically polarized incident signal propagates along one side of the hemisphere wedge scatterer with the electric field tangential to the surface. Since a two-dimensional wedge cannot support such a wave, the VV return predicted by geometrical diffraction theory in Eqs. (13) and (14) is zero. For the actual hemisphere, however, the VV return is finite due to the curvature of the edge and the spherical surface.

Figures 13 and 14 show the leading- and trailing-edge returns obtained from the present method. For HH polarization, the diffraction theory results are also presented. The HH leading-edge return has the 1/kR dependence indicated in Eq. (13a). In addition, the cross section initially decreases and then increases with β as predicted by diffraction theory. However, the magnitude of the cross section is larger than that given by diffraction theory by factors of from 4 to 7. The VV leading-edge return, while not zero, is generally considerably weaker than the HH return. Furthermore, as kR increases and geometric diffraction theory becomes more valid, the VV return decreases more rapidly than the HH return. The β dependence of the VV return is not apparent since the kR dependence changes with β.

The trailing-edge return for HH polarization has a $1/(kR)^2$ dependence rather than 1/kR as predicted by diffraction theory, with both showing an increase of σ with β. The $1/(kR)^2$ dependence is characteristic of doubly-diffracted waves[3] and may reflect a contribution of ray path 5 (see Fig. 10) to the trailing-edge return. Depending on the value of kR, the trailing-edge return is moderately or considerably weaker than predicted by diffraction theory. The VV trailing-edge return is generally comparable to the HH return, decreasing with kR and increasing with β.

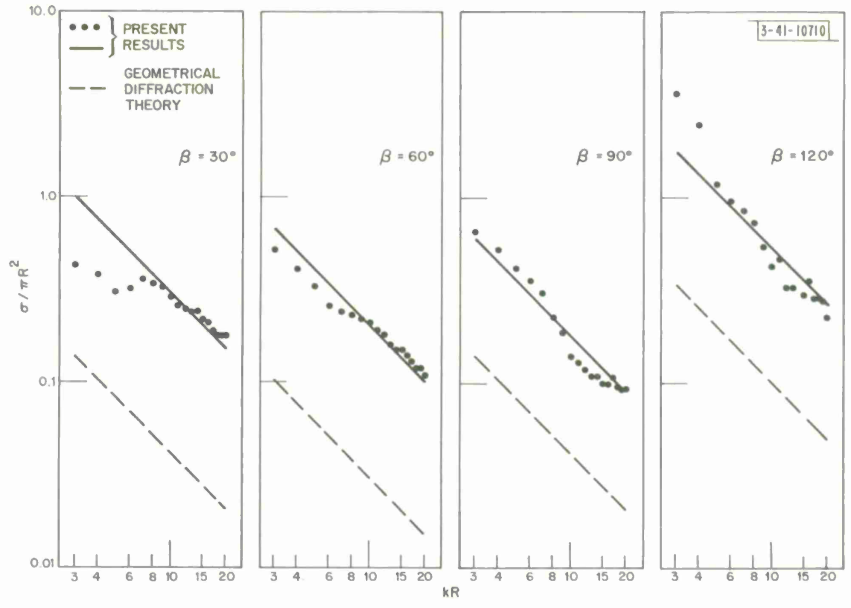

(a)

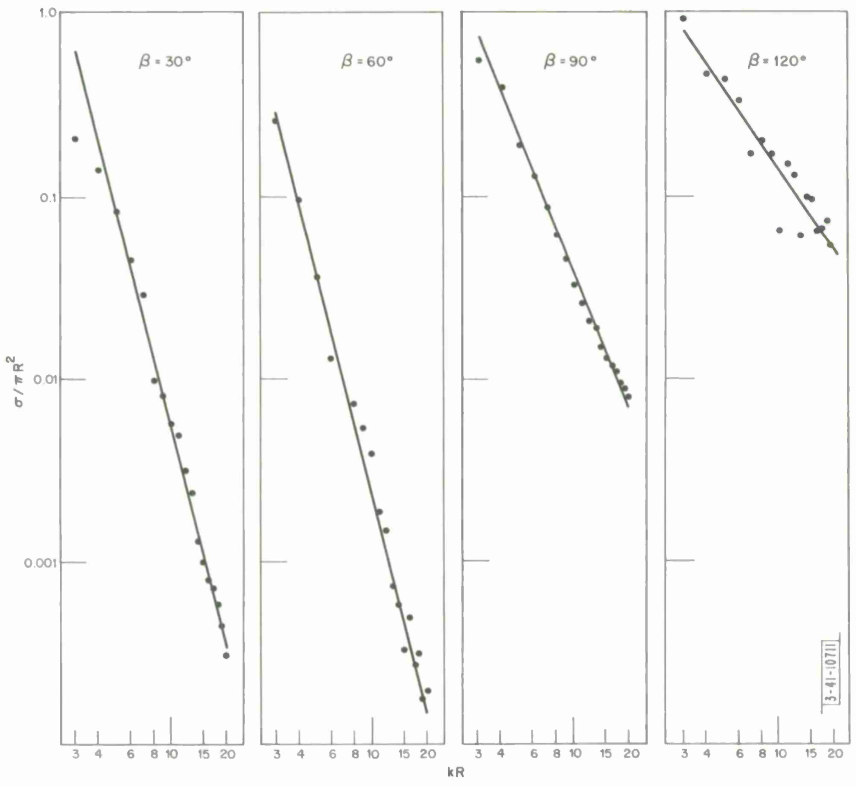

(b)

Fig. 13. Leading edge returns. (a) HH polarization. (b) VV polarization.

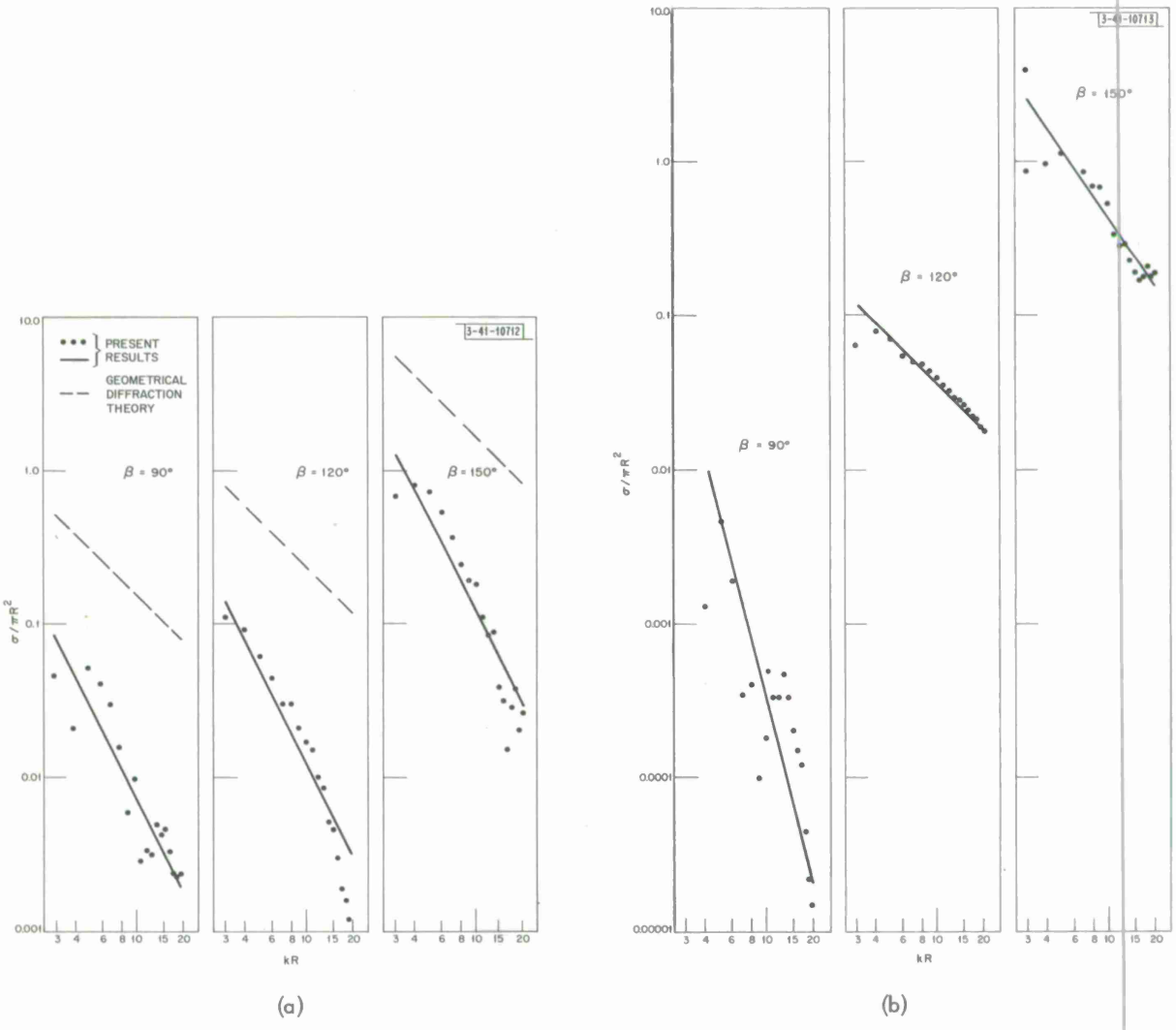

Fig. 14. Trailing edge returns. (a) HH polarization. (b) VV polarization.

TABLE II

CROSS SECTION OF EDGE RETURNS

β	Polarization	$\sigma/\pi R^2$			
		Leading Edge		Trailing Edge	
		Present Results	Diffraction Theory	Present Results	Diffraction Theory
30	HH	$3(kR)^{-1}$	$0.4(kR)^{-1}$	–	–
30	VV	$50(kR)^{-4}$	0	–	–
60	HH	$2(kR)^{-1}$	$0.3(kR)^{-1}$	–	–
60	VV	$23(kR)^{-4}$	0	–	–
90	HH	$1.8(kR)^{-1}$	$0.4(kR)^{-1}$	$0.8(kR)^{-2}$	$1.6(kR)^{-1}$
90	VV	$12(kR)^{-5/2}$	0	$3(kR)^{-4}$	0
120	HH	$5.4(kR)^{-1}$	$1.0(kR)^{-1}$	$1.3(kR)^{-2}$	$2.4(kR)^{-1}$
120	VV	$5(kR)^{-3/2}$	0	$0.35(kR)^{-1}$	0
150	HH	–	$7.2(kR)^{-1}$	$12(kR)^{-2}$	$16(kR)^{-1}$
150	VV	–	0	$14(kR)^{-3/2}$	0

However, its dependence on these parameters is not particularly regular. The kR and β dependence of the various edge returns is summarized in Table II.

It appears that geometrical diffraction theory provides a good qualitative description of the leading-edge return and a fair description of the trailing-edge return for HH polarization. For VV polarization, diffraction theory predicts zero return in disagreement with present results. This behavior may be compared with that of diffraction theory results for backscattering from a flat-backed cone.[10] For HH polarization, diffraction theory is in good agreement with experiment for large kR. For VV polarization, however, the agreement is poor for near nose-on incidence and becomes worse as the cone angle decreases (wedge angle approaches 90°). These results are for long pulse signals and represent combined leading- and trailing-edge returns. For experimental short-pulse backscattering from a flat-backed cone,[12] the leading and trailing edges have been resolved and similar behavior observed. It thus seems that geometrical diffraction theory can provide qualitatively useful results for HH polarization but is of restricted value for VV polarization.

VII. CREEPING-WAVE RETURN

For bistatic scattering, the creeping-wave return considered follows ray path 4 (Fig. 9). The incident signal is diffracted at the trailing edge and a surface wave launched. This wave propagates along the surface of the hemisphere for a distance $R\beta$ and then radiates toward the

receiver. To calculate the amplitude of this creeping-wave return, it is necessary to determine the edge diffraction coefficient for launching the creeping wave, the attenuation of this wave as it propagates, and finally, the radiation coefficient in the direction of scattering. The diffraction coefficient should only depend on kR and not on β for nose-on incidence. The propagation and radiation effects should be identical with the known results for creeping waves on spheres. We shall restrict our consideration to the case of HH polarization since the VV creeping-wave returns were generally weaker and less reliable. The β dependence of this return may be obtained from the leading term in the creeping-wave return for a sphere[13]

$$\sigma_{HH}(\beta) \sim \frac{1}{\sin\beta} \exp\left[-1.02(kR/2)^{1/3}\,\beta\right] \quad . \tag{15}$$

All factors independent of β have been ignored in Eq. (15). A comparison of present results with Eq. (15) for kR = 10 is shown in Fig. 15, where $\sigma \sin\beta/\pi R^2$ is plotted as a function of β. The agreement seems good although not conclusive. By writing

$$\frac{\sigma_{HH}}{\pi R^2} = \frac{F(kR)}{\sin\beta} \exp\left[1.02(kR/2)^{1/3}\,\beta\right] \tag{16}$$

and finding the best estimate of F for each value of kR, we may obtain the dependence of the edge diffraction coefficient on kR. This has been done but the results are inconclusive. There appears to be a slight decrease in F(kR) with increasing kR, but fluctuations in the observed values of F are substantially greater than this systematic decrease. The values of F(kR) in Eq. (16) generally fall between 0.02 and 0.2.

While the creeping-wave return can be resolved and identified, it appears to be too weak to permit accurate measurement and thus, extrapolation to other targets. The results obtained are in reasonable agreement with creeping-wave theory but are not sufficiently reliable to permit any more definitive statements.

The doubly-diffracted returns (ray paths 5 through 10), while occasionally observed in the short-pulse response, are generally weaker than the creeping-wave return and are ignored in this report.

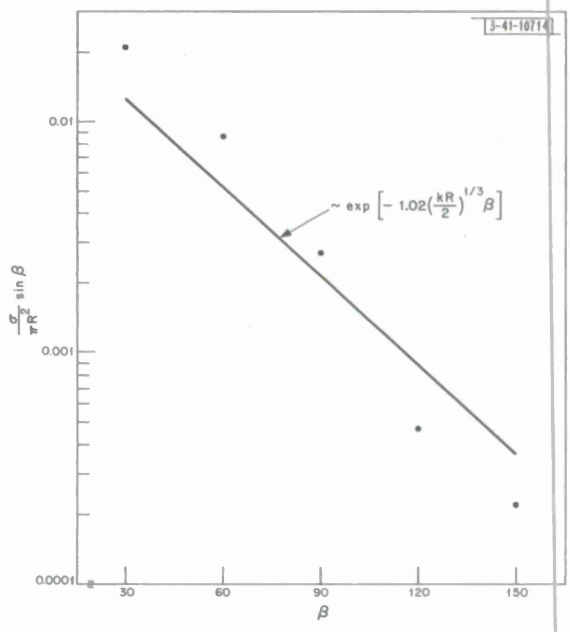

Fig. 15. Creeping-wave return vs bistatic angle; kR = 10, HH polarization.

VIII. CONCLUSIONS

In this report, the electromagnetic scattering from a conducting hemisphere at nose-on incidence has been considered from a short-pulse viewpoint. The CW scattering amplitude was calculated as a function of frequency, bistatic angle, and polarization. From this information, the short-pulse response was constructed by Fourier synthesis. This permitted resolution and identification of individual contributions of each scattering center having different ray path lengths. The more important of these returns were then isolated and investigated in more detail to determine their frequency, bistatic angle, and polarization dependence. For bistatic scattering, the specular, leading- and trailing-edge diffraction and creeping-wave returns were considered. Doubly-diffracted waves were discussed briefly for bistatic scattering but were considered in more detail for backscattering. Results obtained for individual returns were compared with other appropriate theoretical predictions; qualitative and some quantitative agreement was observed.

Of particular interest was the comparison of the edge returns with those calculated using geometrical diffraction theory. For HH polarization (E-plane scattering), geometrical diffraction theory provides a good qualitative estimate of the frequency and angle dependence of edge scattering, although the numerical results differ by a factor of about five (geometrical diffraction theory results are too small). For VV polarization (H-plane scattering), Keller's geometrical diffraction theory predicts zero edge scattering, while the observed scattering is finite. This is not unexpected since diffraction theory has been shown to be poor for VV polarization for other targets.

The bistatic scattering results presented here are of interest primarily for comparison with results of approximate theory and this has been emphasized in the report. For application to scattering from other targets (for example, the edge of a finite cylinder), it would be desirable to extend the present results to off nose-on incidence. This extension is straightforward in principle, but in practice, would be quite difficult.

REFERENCES

1. T.B.A. Senior, "The Backscattering Cross Section of a Cone-Sphere," IEEE Trans. AP-13, 271 (March 1965).
2. J.H. Pannell, J. Rheinstein and A.F. Smith, "Radar Scattering from a Conducting Cone-Sphere," Technical Report 349, Lincoln Laboratory, M.I.T. (2 March 1964).
3. J.B. Keller, "Backscattering from a Finite Cone," IRE Trans. AP-8, 175 (March 1960).
4. E.M. Kennaugh, "The Scattering of Plane Electromagnetic Waves by a Perfectly Conducting Hemisphere or Hemispherical Shell," Ohio State U. Antenna Lab. Project Report 302-35 (15 May 1950).
5. R.W.P. King and T.T. Wu, The Scattering and Diffraction of Waves (Harvard Univ. Press, 1959).
6. W.E. Blore and H.M. Musal, "The Radar Cross Section of Metal Hemispheres, Spherical Segments, and Partially Capped Spheres," IEEE Trans. AP-13, 478 (May 1965).
7. J. Rheinstein, "Scattering of Short Pulses of Electromagnetic Waves," Proc. IEEE 53, 1069 (August 1965).
8. _____, "Backscatter from Spheres; A Short Pulse View," Technical Report 414, Lincoln Laboratory, M.I.T. (27 April 1966).
9. J.B. Keller, "Diffraction by an Aperture," J. Appl. Phys. 28, 426 (April 1957).
10. M.E. Bechtel, "Application of Geometric Diffraction Theory to Scattering from Cones and Disks," Proc. IEEE 53, 877 (August 1965).
11. R.F. Goodrich, B.A. Harrison, R.E. Kleinman and T.B.A. Senior, "Studies in Radar Cross Sections XLVII – Diffraction and Scattering by Regular Bodies – I: The Sphere," U. of Mich. Rad. Lab. Report 3648-1-T (December 1961).
12. S. Hong and S.L. Borison, "Short-Pulse Scattering by a Cone – Direct and Inverse," to be published in IEEE Trans. on Ant. and Prop.
13. T.B.A. Senior and R.F. Goodrich, "Scattering by a Sphere," Proc. IEE 111, 907 (May 1964).

DOCUMENT CONTROL DATA – R&D

(Security classification of title, body of abstract and indexing annotation must be entered when the overall report is classified)

1. ORIGINATING ACTIVITY *(Corporate author)* Lincoln Laboratory, M.I.T.	2a. REPORT SECURITY CLASSIFICATION Unclassified 2b. GROUP None

3. REPORT TITLE

Short-Pulse Scattering by a Hemisphere

4. DESCRIPTIVE NOTES *(Type of report and inclusive dates)*
Technical Report

5. AUTHOR(S) *(Last name, first name, initial)*

Weiner, Stephen D.

6. REPORT DATE 18 July 1967	7a. TOTAL NO. OF PAGES 24	7b. NO. OF REFS 13
8a. CONTRACT OR GRANT NO. AF 19 (628)-5167 b. PROJECT NO. Order 498 c. d.	9a. ORIGINATOR'S REPORT NUMBER(S) Technical Report 436 9b. OTHER REPORT NO(S) *(Any other numbers that may be assigned this report)* ESD-TR-67-331	

10. AVAILABILITY/LIMITATION NOTICES

This document has been approved for public release and sale; its distribution is unlimited.

11. SUPPLEMENTARY NOTES None	12. SPONSORING MILITARY ACTIVITY Advanced Research Projects Agency, Department of Defense

13. ABSTRACT

The radar scattering by a conducting hemisphere for incidence along the symmetry axis has been determined as a function of frequency, bistatic angle, and polarization. From this frequency domain information, the short-pulse response is constructed using Fourier synthesis. The range resolution thus afforded permits identification of various contributions to the scattering – in particular, that due to edge diffraction. Results obtained from the geometrical theory of diffraction are in qualitative agreement with those obtained here.

14. KEY WORDS

short-pulse scattering
radar scattering
short-pulse response
conducting hemisphere
cw scattering
scattering by hemispheres
range resolution
geometrical theory of diffraction
edge diffraction
electromagnetic scattering
bistatic scattering
ray paths

Printed by
United States Air Force
L. G. Hanscom Field
Bedford, Massachusetts